Physics of Fluids

RESEARCH ARTICLE | JUNE 01 2022

Helicity budget in turbulent channel flows with streamwise rotation

Zheng Yan (闫政) ; Xinliang Li (李新亮) ; Changping Yu (于长平) ✉

Physics of Fluids 34, 065105 (2022)
https://doi.org/10.1063/5.0094910

Physics of Fluids ARTICLE scitation.org/journal/phf

Helicity budget in turbulent channel flows with streamwise rotation

Cite as: Phys. Fluids **34**, 065105 (2022); doi: 10.1063/5.0094910
Submitted: 6 April 2022 · Accepted: 19 May 2022 ·
Published Online: 1 June 2022

Zheng Yan (闫政),[1] Xinliang Li (李新亮),[2,3] and Changping Yu (于长平)[2,3,a)]

AFFILIATIONS

[1]Institute of Applied Physics and Computational Mathematics, Beijing 100094, China
[2]LHD, Institute of Mechanics, Chinese Academy of Sciences, Beijing 100190, China
[3]School of Engineering Science, University of Chinese Academy of Sciences, Beijing 100049, China

[a)]Author to whom correspondence should be addressed: cpyu@imech.ac.cn

ABSTRACT

The streamwise rotation effects in turbulent channel flows are reflected not only in the appearance of the secondary flows but also in the weakened streamwise velocity and spanwise vorticity. In this paper, we investigate the secondary flows from three perspectives: the mean spanwise velocity, the mean streamwise vorticity, and combined mean and fluctuating helicity. We found that the combined helicity is also an alternative perspective to characterize the streamwise rotation effect, especially for the secondary flows. The budget equations of the mean and fluctuating helicity in physical space are derived theoretically and analyzed numerically. The streamwise rotation effects on the secondary flows are directly reflected on the pressure and Coriolis terms, which provides an essential source for helicity within the near-wall regions. The production term could be decomposed into two terms, which originate from the momentum and vorticity equations, respectively. The helical stress (velocity–vorticity correlation) originating from the vorticity equation shows a simple profile distribution and is dominant for the production for the helicity within the near-wall regions. The high helical structures in the core regions can be explained as an intense wall-normal transportation, which transfers produced helicity within the near-wall regions into the core regions.

I. INTRODUCTION

Turbulent flows subjected to system rotation are common in natural and engineering applications, such as the Ekman layer in atmospheric flows and turbomachinery.[1–5] The flow characters are significantly affected by the appearance of system rotation, depending on the rotating directions.[2,3] In the past few decades, many efforts had been devoted to turbulent boundary layers with streamwise,[6–10] wall-normal,[5,11–13] and spanwise rotations.[14–19] Yang and Wang[8] studied the Taylor–Görtler vortices at high rotation numbers in turbulent channel flows with streamwise rotation and confirmed the two-layer pattern of Taylor–Görtler vortices. Deusebio and Lindborg[5] investigated the Ekman boundary layer through the incompressible boundary layer with wall-normal rotation and confirmed the helicity cascade in the logarithmic range. Xia *et al.*[16] carried out a series of direct numerical simulations (DNS) of turbulent channel flows with spanwise rotation and identified the linear profile of the streamwise velocity fluctuations, the Reynolds shear stress.

In addition to the DNS, the large-eddy simulations (LES) of the turbulent channel flows with the streamwise rotation are also carried out, and the numerical results show good quantitative agreements with those of DNS.[3,9,20–26] Dai *et al.*[9] studied the turbulent channel flows with streamwise rotation with high Reynolds numbers through LES and found that the streamwise rotation promotes the cylones and suppresses the anti-cylones. Huang and Yang[21] established the mean flow scaling for wall-bounded flows and carried out wall-modeled LES with high Reynolds numbers. Wang and Zhang[24] used two dynamic subgrid-scale stress models and two dynamic subgrid-scale heat flux models to perform LES of turbulent flows in a heated streamwise rotating channel and explored the subgrid-scale effects on the budget balance of turbulent stresses and heat fluxes.

The secondary flows would present in turbulent channel flows with streamwise rotation, and it is directly reflected on the appearance of the mean spanwise velocity with "double S-shaped" profiles.[6,27,28] The secondary flows also exist in other flows, such as curved pipes (the first-kind Prandtl's secondary flows)[29–31] and duct flows (the second-kind Prandtl's secondary flows).[32–34] Moreover, the existence of the mean streamwise vorticity is also an important characteristic of the secondary flows,[1] which corresponds to the wall-normal gradient of the mean spanwise velocity. However, the system rotation effects are also reflected in other aspects, such as decreased mean streamwise

velocity and mean spanwise vorticity in the core regions. Moreover, the rotation number effects are non-monotonous, which is complex to characterize the three-dimensional effects in a rotating system. Our previous study revealed that helicity (the scalar product of the velocity and vorticity) is an alternative comprehensive representation of the system rotation effects,[10] including the secondary flows and dominant velocity and vorticity. This conclusion had been validated in turbulent channel flows with streamwise rotation and the duct flows. As one of the only two quadratic inviscid invariances in three-dimensional turbulent flows, the research of helicity uncovers new physical processes of the system evolutions,[35–38] such as vortex morphology,[39–41] helical turbulent structures for scalar transport,[42] inverse energy cascade,[43–45] etc. Some statistical regulations had been extended to compressible turbulent flows.[46–48]

The origin and sustaining mechanisms of the secondary flows could be investigated through the budget of the Reynolds stresses. The main reason lies in the fact that only Reynolds stresses are present in the governing equation of the mean spanwise velocity [Eq. (5)], in addition to the viscous dissipation term. The budget of Reynolds stresses has been used to explore the origin and the sustaining mechanism in turbulent channel flows with streamwise rotation in physical space[8,28] and spectral space.[49] Yang *et al.*[28] found that the production term of the budget of the Reynolds stress provides negative feedback, which is used to non-monotonous regulations of the rotation numbers. The methodology of the budget analysis of the Reynolds stresses has also been applied to other flows.[14,50–53] Kawata and Alfredsson[52] proposed that the Reynolds shear stress is transferred from the small-scale near-wall structures into the large scales away from the wall in plane Couette flows, and this conclusion is further studied in zero-pressure-gradient boundary layers.[53] These studies provided many important theoretical suggestions for the Reynolds-averaged Navier–Stokes equations (RANS) models.

Our previous work used helicity to characterize the flow structures through profile distribution, scale distribution, and inter-scale interaction.[10] In this paper, we extend the methodology of the Reynolds stress budget to mean and fluctuate helicity budgets, to investigate the system rotation effects on flow evolutions. The rest of this paper is organized as follows. In Sec. II, we introduce the database of the turbulent channel flows with streamwise rotation we performed previously.[10] In Sec. III, we analyze the budget of secondary flows from the perspective of the mean spanwise velocity, the mean streamwise vorticity, and the mean and fluctuating helicity. Finally, we summarize main conclusions in Sec. IV.

II. DATABASE OF THE TURBULENT CHANNEL FLOWS WITH STREAMWISE ROTATION

In our previous work, we performed DNS of the turbulent channel flows with streamwise rotation with different rotation numbers and Reynolds numbers.[10] The governing equations are the incompressible Navier–Stokes equations in a rotating reference frame,[54]

$$\frac{\partial u_i}{\partial t} + u_k \frac{\partial u_i}{\partial x_k} = -\frac{1}{\rho}\frac{\partial p}{\partial x_i} + \nu \frac{\partial^2 u_i}{\partial x_k \partial x_k} - 2\varepsilon_{ijk}\Omega_j u_k - \frac{\Pi}{\rho}\delta_{i1}, \quad (1a)$$

$$\frac{\partial u_i}{\partial x_i} = 0, \quad (1b)$$

where $\mathbf{u}$ is the velocity vector, ρ is the density, p is the modified total pressure, and $\mathbf{\Omega}$ is the rotating vector of the system rotation with

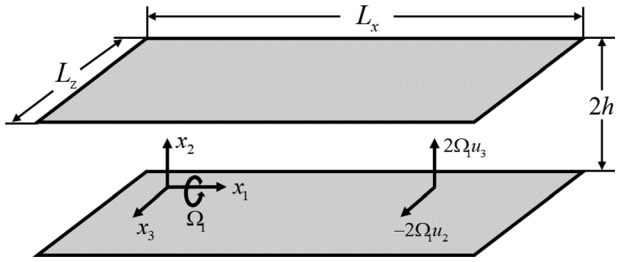

FIG. 1. Schematic of the turbulent channel flows with streamwise rotation.

$\mathbf{\Omega} = (\Omega_1, 0, 0)$. ν is the kinematic viscosity, and $\nu = \mu/\rho$. Here, μ is the dynamic viscosity. The constant mean streamwise pressure gradient $\frac{\Pi}{\rho}\delta_{i1}$ is used to driving the channel flows, and δ_{ij} is Kronecker's delta. The above equations are numerically resolved in a Cartesian coordinate with streamwise (x), wall-normal (y), and spanwise (z) directions. For the convenience of theoretical derivation, the streamwise, wall-normal, and spanwise directions are also marked as x_1, x_2, and x_3, respectively. Fourier series are used in the horizontal directions with periodic boundary conditions, and Chebyshev polynomials are used in the wall-normal direction with non-slip and impermeable boundary conditions.[7,8,55] The computational configuration are shown schematically in Fig. 1.

The key information of the numerical simulations is listed in Table I. The Reynolds number based on the friction velocity is defined as $Re_\tau = hu_\tau/\nu$, where u_τ is the mean wall-friction velocity. The rotation number based on the friction velocity is defined as $Ro_\tau = 2\Omega h/u_\tau$. In the subsequent numerical analysis, the focused physical variables are non-dimensionalized by inner scales, including the friction velocity u_τ and the viscous length scale $\delta = \nu/u_\tau$. The current computational domains are sufficient to capture some key information of flow structures,[8] with corresponding rotation numbers.

III. RESULTS AND DISCUSSION

The secondary flows in turbulent channel flows with streamwise rotation could be characterized by the presence of the mean spanwise velocity and streamwise vorticity.[1,3,6,27] Our previous study revealed that the helicity is a combined result of the system rotation's affected directional velocities and vorticities, including the secondary flows.[10] This section compares three methods characterizing the secondary flows, including the mean spanwise velocity, the mean streamwise vorticity, and mean and fluctuating helicity. Their governing equations are derived and estimated numerically by the database of the turbulent

TABLE I. The computational domains, grid settings, and key parameters. L_x is the streamwise computational length, L_z is the spanwise computational length, and h is the half-channel height, which is set to be 1. N_x denotes the streamwise grid, N_y denotes the wall-normal grid, and N_z denotes the spanwise grid.

Case	$L_x \times 2h \times L_z$	$N_x \times N_y \times N_z$	Re_τ	Ro_τ
ST07	$32\pi \times 2 \times 8\pi$	$1024 \times 128 \times 512$	180	7.5
ST07R	$32\pi \times 2 \times 8\pi$	$4096 \times 192 \times 1536$	395	7.5
ST15	$64\pi \times 2 \times 8\pi$	$2048 \times 128 \times 512$	180	15
ST30	$128\pi \times 2 \times 8\pi$	$4096 \times 128 \times 512$	180	30

channel flows with streamwise rotation with different rotation numbers and Reynolds numbers.

A. The mean spanwise velocity

The first highlighted physical variable characterizing the secondary flows is the mean spanwise velocity. The velocity field can be decomposed into mean and fluctuating components as $\mathbf{u} = \langle \mathbf{u} \rangle + \mathbf{u}'$, where $\langle \cdot \rangle$ denotes the ensemble average over the streamwise and spanwise planes and time. Their governing equations could be derived as follows:

$$\frac{\partial \langle u_i \rangle}{\partial t} + \langle u_j \rangle \frac{\partial \langle u_i \rangle}{\partial x_j} = -\frac{1}{\rho}\frac{\partial \langle p \rangle}{\partial x_i} - 2\varepsilon_{ikl}\Omega_k \langle u_l \rangle + \nu \frac{\partial^2 \langle u_i \rangle}{\partial x_j \partial x_j} - \frac{\partial \langle u_i' u_j' \rangle}{\partial x_j} - \frac{\Pi}{\rho}\delta_{i1}, \quad (2)$$

$$\frac{\partial u_i'}{\partial t} + \langle u_j \rangle \frac{\partial u_i'}{\partial x_j} + u_j' \frac{\partial \langle u_i \rangle}{\partial x_j} = -\frac{1}{\rho}\frac{\partial p'}{\partial x_i} - 2\varepsilon_{ikl}\Omega_k u_l' + \nu \frac{\partial^2 u_i'}{\partial x_j \partial x_j} - \frac{\partial}{\partial x_j}(u_i' u_j' - \langle u_i' u_j' \rangle). \quad (3)$$

The spatial homogeneity in the streamwise and spanwise directions leads to a zero mean gradient, and it is expressed as

$$\frac{\partial}{\partial x_1}\langle \cdot \rangle = \frac{\partial}{\partial x_3}\langle \cdot \rangle = 0. \quad (4)$$

Hence, the governing equation of the mean spanwise velocity with a steady state could be expressed as

$$\frac{\partial \langle u_3 \rangle}{\partial t} = 0 = \nu \frac{\partial^2 \langle u_3 \rangle}{\partial x_k \partial x_k} - \frac{\partial \langle u_2' u_3' \rangle}{\partial x_2}. \quad (5)$$

It is concluded that the mean spanwise velocity directly originates from the wall-normal gradient of Reynolds stress $\langle u_2' u_3' \rangle$, rather than the mean Coriolis and pressure terms.[5,28] The numerical results of the mean spanwise velocity $\langle u_3 \rangle$ with different rotation numbers and Reynolds numbers are shown in Fig. 2. The reverse spanwise flows are present in the core regions, which characterizes the secondary flows in the turbulent channel flows with streamwise rotation. Consistent with previous works,[7,8,28] the mean spanwise velocity within the near-wall regions increases with the rotation numbers, while it shows a non-monotonous regulation in the core regions. The effect of the Reynolds number on the mean near-wall spanwise velocity is negligible. Nevertheless, the magnitude of the mean spanwise velocity increases with Reynolds numbers above the buffer layer.

As an origin of the mean spanwise velocity, Reynolds stress $\langle u_2' u_3' \rangle$ plays an essential role in the secondary flows, and we show the numerical results with different rotation numbers and Reynolds numbers in Fig. 3. Their magnitudes are small within the viscous sublayer, meaning that the viscous dissipation process might be dominant within the viscous sublayer. Over the viscous sublayer, their magnitudes increase to peak values and then decrease monotonously. The locations of their maxima are consistent with the locations of the maximum mean spanwise velocities in Fig. 2. The corresponding relation indicates that the Reynolds stress $\langle u_2' u_3' \rangle$ is crucial for the evolution of the mean spanwise velocity. With the increase in the rotation numbers, the magnitudes of the Reynolds stress $\langle u_2' u_3' \rangle$ increase, and their

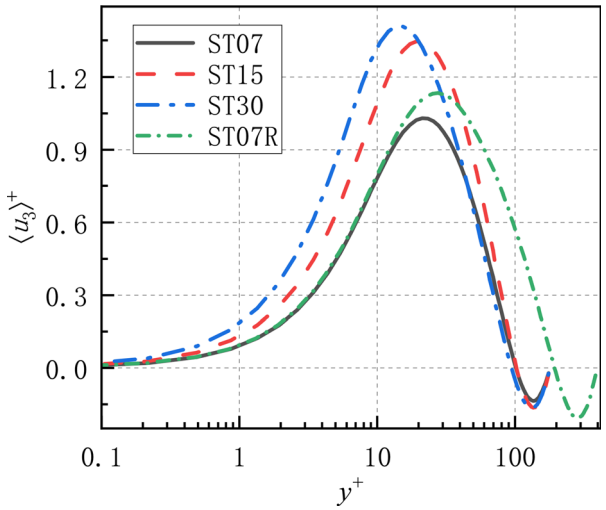

FIG. 2. Profiles of the mean spanwise velocity $\langle u_3 \rangle$ with different rotation numbers and Reynolds numbers.

wall-normal gradients also increase. This phenomenon could be used to explain the rotation number effects on the strength of the secondary flows within the near-wall regions in Fig. 2. Moreover, the starting and peak locations of the large Reynolds stress $\langle u_2' u_3' \rangle$ are approaching the wall, corresponding to the rotation number effects on the peak locations of the secondary flows. As for the Reynolds number effect, it has a negligible influence on the Reynolds stress $\langle u_2' u_3' \rangle$ within the near-wall regions and increases the regions of the positive spanwise velocity.

Although the governing equation of the mean spanwise velocity [Eq. (5)] indicates that the secondary flows are not associated with the Coriolis term directly, the secondary flows exist only when the Coriolis is present. To uncover the Coriolis effect on the

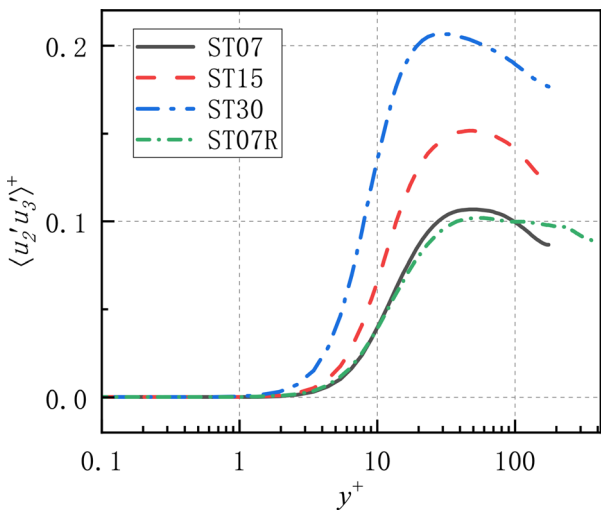

FIG. 3. Profiles of the Reynolds stress $\langle u_2' u_3' \rangle$ with different rotation numbers and Reynolds numbers.

secondary flows, we derive the general Reynolds stress equations as follows:[8,50,51,53,56]

$$\frac{\partial\langle u_i'u_j'\rangle}{\partial t}+\langle u_k\rangle\frac{\langle u_i'u_j'\rangle}{\partial x_k}$$
$$=\underbrace{-\langle u_i'u_k'\rangle\frac{\partial\langle u_j\rangle}{\partial x_k}-\langle u_j'u_k'\rangle\frac{\partial\langle u_i\rangle}{\partial x_k}}_{P_{ij}^R}+\underbrace{\left\langle\frac{p'}{\rho}\left(\frac{\partial u_j'}{\partial x_i}+\frac{\partial u_i'}{\partial x_j}\right)\right\rangle}_{\Phi_{ij}^R}$$
$$\underbrace{-2\varepsilon_{ikl}\Omega_k\langle u_l'u_j'\rangle-2\varepsilon_{jkl}\Omega_k\langle u_l'u_i'\rangle}_{C_{ij}^R}\underbrace{-2\nu\left\langle\frac{\partial u_i'}{\partial x_k}\frac{\partial u_j'}{\partial x_k}\right\rangle}_{D_{ij}^R}$$
$$\underbrace{-\frac{\partial}{\partial x_k}\left(\frac{1}{\rho}\left(\langle p'u_i'\delta_{jk}\rangle+\langle p'u_j'\delta_{ik}\rangle\right)+\langle u_i'u_j'u_k'\rangle-\nu\frac{\partial\langle u_i'u_j'\rangle}{\partial x_k}\right)}_{T_{ij}^R},\tag{6}$$

where P_{ij}^R is the production term, and it represents the interaction between the mean and fluctuating fields. Φ_{ij}^R is the pressure-velocity correlation term, and it represents the coupling of the fluctuating pressure and velocity gradients. C_{ij}^R is the Coriolis term, which denotes the effect of the system rotation. D_{ij}^R is the viscous dissipation term. T_{ij}^R is the spatial transportation term. The governing equation of the highlighted Reynolds stress $\langle u_2'u_3'\rangle$ could be obtained from Eq. (6). From the above equation, we can find that the Coriolis term C_{23}^R for the Reynolds stress $\langle u_2'u_3'\rangle$ is non-zero. It could be conclude that the Coriolis term affects the evolution of the Reynolds stress $\langle u_2'u_3'\rangle$ and then dominates the evolution of the secondary flows. In addition, the Coriolis effect is also involved in the pressure term.[28,57]

We show the numerical statistical consequences of the budget of the Reynolds stress $\langle u_2'u_3'\rangle$ with different rotation numbers and Reynolds numbers in Fig. 4. There exist three zero points of the profile of the production term P_{23}^R within a half channel, and it is regarded as an alternative explanation for the non-monotonous regulations of the rotation number effects.[28] According to the definition of the production term P_{23}^R, its sign depends on the wall-normal gradient of the mean spanwise velocity, and the numerical results in Fig. 4 confirm this explanation. The large wall-normal gradient of the spanwise velocity leads to a larger magnitude of the production term between the viscous sublayer and core regions, and it serves as a sink role within these regions. The Coriolis term C_{23}^R makes a dominant contribution around the peak location of

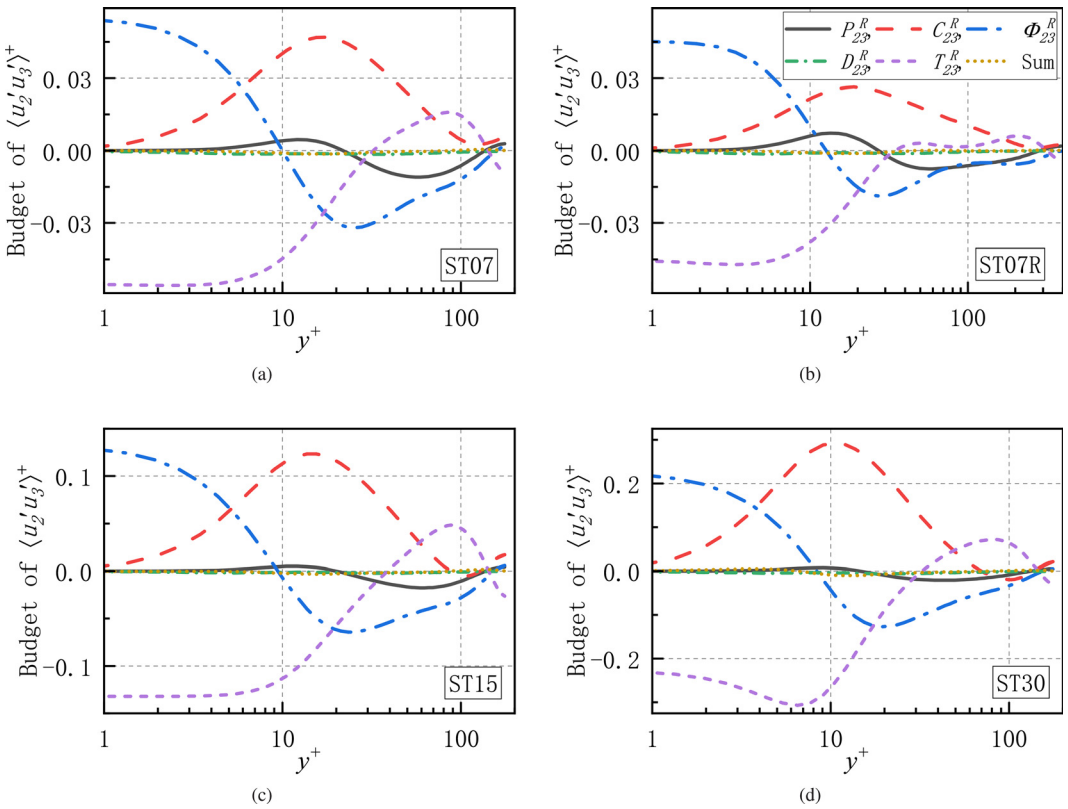

FIG. 4. Profiles of the budget terms of the Reynolds stress $\langle u_2'u_3'\rangle$ with different rotation numbers and Reynolds numbers. (a) ST07, (b) ST07R, (c) ST15, and (d) ST30. All budget terms are non-dimensionalized by u_τ^3/δ according to their dimensions.

the Reynolds stress $\langle u_2' u_3' \rangle$, and the associated pressure term Φ_{23}^R is dominant within the near-wall regions. The contribution of the viscous dissipation term D_{23}^R is negligible. The rotation number effects are represented on the larger magnitudes and smaller peak locations, similar to that of the mean spanwise velocity. With a higher Reynolds number, the magnitude of the production term is larger, and the magnitudes of other budget terms are smaller. The larger magnitude of the production term originates from the strengthened mean spanwise velocity, which shows a larger wall-normal gradient of the mean spanwise velocity in Fig. 2.

B. The mean streamwise vorticity

The mean streamwise vorticity is also employed to represent the secondary flows. The general mean and fluctuating vorticity equations are obtained by making a curl operation on Eqs. (2) and (3), and they are

$$\frac{\partial \langle \omega_i \rangle}{\partial t} + \langle u_j \rangle \frac{\partial \langle \omega_i \rangle}{\partial x_j} = \langle \omega_j \rangle \frac{\partial \langle u_i \rangle}{\partial x_j} + \nu \frac{\partial^2 \langle \omega_i \rangle}{\partial x_j \partial x_j} + 2\Omega_j \frac{\partial \langle u_i \rangle}{\partial x_j} - \frac{\partial \left(\langle \omega_i' u_j' \rangle - \langle u_i' \omega_j' \rangle \right)}{\partial x_j}, \quad (7)$$

$$\frac{\partial \omega_i'}{\partial t} + \langle u_j \rangle \frac{\partial \omega_i'}{\partial x_j} + u_j' \frac{\partial \langle \omega_i \rangle}{\partial x_j} = \langle \omega_j \rangle \frac{\partial u_i'}{\partial x_j} + \omega_j' \frac{\partial \langle u_i \rangle}{\partial x_j} + 2\Omega_j \frac{\partial u_i'}{\partial x_j} + \nu \frac{\partial^2 \omega_i'}{\partial x_j \partial x_j} - \frac{\partial}{\partial x_j} \left(\langle u_i' \omega_j' \rangle - u_i' \omega_j' - \left(\langle \omega_i' u_j' \rangle - \omega_i' u_j' \right) \right). \quad (8)$$

In the turbulent channel flows with streamwise rotation, the mean streamwise vorticity corresponds to the wall-normal gradient of the mean spanwise velocity, and it is expressed as

$$\langle \omega_1 \rangle = \frac{\partial \langle u_3 \rangle}{\partial x_2} - \frac{\partial \langle u_2 \rangle}{\partial x_3} \equiv \frac{\partial \langle u_3 \rangle}{\partial x_2}. \quad (9)$$

Its governing equation with a steady state reads as

$$\frac{\partial \langle \omega_1 \rangle}{\partial t} = 0 = \nu \frac{\partial^2 \langle \omega_1 \rangle}{\partial x_j \partial x_j} - \frac{\partial \gamma}{\partial x_2}, \quad (10)$$

where $\gamma = \langle \omega_1' u_2' \rangle - \langle u_1' \omega_2' \rangle$. Similar to Reynolds stress's definition, there is a mean velocity–vorticity correlation term involved in the governing equation of the mean streamwise vorticity, which serves as a sustaining mechanism for the secondary flows. The numerical consequences of the mean streamwise vorticity $\langle \omega_1 \rangle$ and the mean velocity–vorticity correlation γ are shown in Figs. 5 and 6, respectively. The profile distributions of the mean streamwise vorticity are consistent with the mean spanwise velocity in Fig. 2, and the rotation number effects are represented on the larger magnitudes of the mean streamwise vorticity. In contrast to the profile distribution of the Reynolds stress $\langle u_2' u_3' \rangle$ in Fig. 3, the profile distributions of the velocity–vorticity correlation γ in Fig. 6 show a simple regulation. With the increase in the wall-normal distance, the magnitude of the velocity–vorticity correlation γ begins to increase to a peak value around the buffer layer and then decrease to a small value. The peak

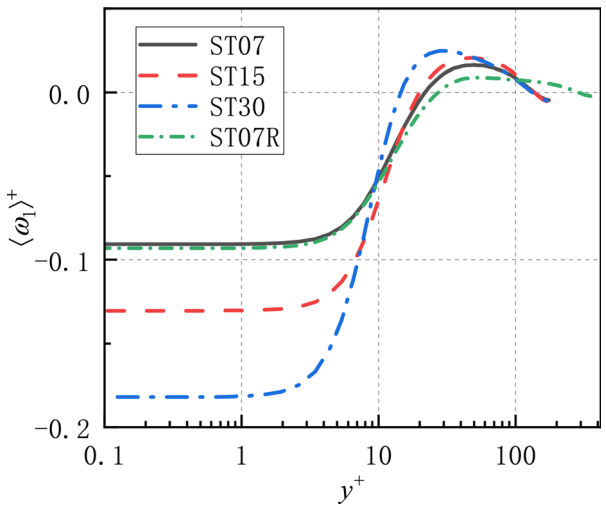

FIG. 5. Profiles of the mean streamwise vorticity $\langle \omega_1 \rangle$ with different rotation numbers and Reynolds numbers.

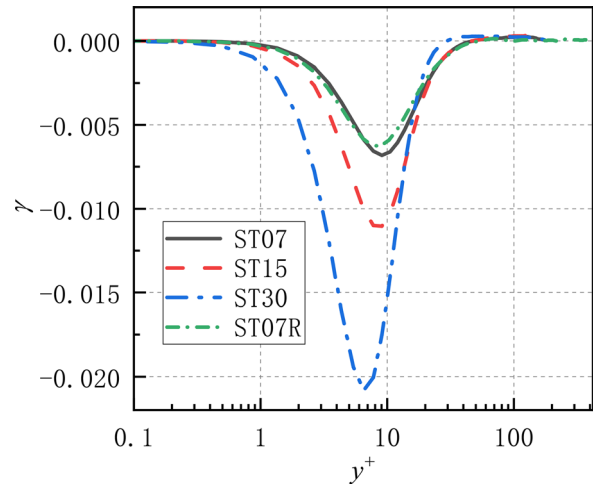

FIG. 6. Profiles of the mean velocity–vorticity correlation γ with different rotation numbers and Reynolds numbers.

location is more approaching the wall, contrast to the Reynolds stress $\langle u_2' u_3' \rangle$ in Fig. 3. The rotation number effects are also represented on the larger magnitudes and smaller peak location values.

The general velocity–vorticity correlation can be expanded as

$$\langle u_i \omega_j \rangle = \left(\langle u_i \rangle + u_i' \right) \cdot \left(\langle \omega_j \rangle + \omega_j' \right) \equiv \langle u_i \rangle \langle \omega_j \rangle + \langle u_i' \omega_j' \rangle. \quad (11)$$

The governing equations of the above mean and fluctuating components are given in Appendix.

The governing equation of the mean velocity–vorticity correlation γ can be obtained from Eq. (12), which is

$$\frac{\partial \gamma}{\partial t} = \underbrace{-\langle u_2' u_2' \rangle \frac{\partial \langle \omega_1 \rangle}{\partial x_2}}_{P^\gamma} \underbrace{-\frac{1}{\rho}\left\langle \frac{\partial p'}{\partial x_2}\omega_1' - \frac{\partial p'}{\partial x_1}\omega_2' \right\rangle}_{\Phi^\gamma} + \underbrace{2\Omega_1 \left\langle u_3'\omega_1' + u_2' \frac{\partial u_1'}{\partial x_1} - u_1' \frac{\partial u_2'}{\partial x_1} \right\rangle}_{C^\gamma} \underbrace{-2\nu \left\langle \frac{\partial u_2'}{\partial x_k}\frac{\partial \omega_1'}{\partial x_k} - \frac{\partial u_1'}{\partial x_k}\frac{\partial \omega_2'}{\partial x_k} \right\rangle}_{D^\gamma}$$
$$\underbrace{-\frac{\partial}{\partial x_2}\left(\langle u_2'(\omega_1' u_2' - \omega_2' u_1') \rangle - \nu \frac{\partial \gamma}{\partial x_2} \right) + \left\langle \omega_k' \left(u_2' \frac{\partial u_1'}{\partial x_k} - u_1' \frac{\partial u_2'}{\partial x_k} \right) \right\rangle + \langle \omega_k \rangle \left\langle u_2' \frac{\partial u_1'}{\partial x_k} - u_1' \frac{\partial u_2'}{\partial x_k} \right\rangle}_{T^\gamma}, \quad (k = 1, 2, 3). \tag{12}$$

The budget terms with different rotation numbers and Reynolds numbers are shown in Fig. 7. In contrast to the role of the production term for the Reynolds stress $\langle u_2' u_3' \rangle$, the production term P^γ serves as a pure sink role for the mean velocity–vorticity correlation γ. Another source term within the near-wall regions is the Coriolis term C^γ. However, the pressure term Φ^γ is complex. It plays a sink role within the near-wall regions and plays a source role above the buffer layer. The magnitudes of the transportation term T^γ are relatively large, and only 10% are shown for comparison with other terms. Below the core region, transportation always serves as a sink role. It means that the wall-normal flux is very large. It transports the mean velocity–vorticity correlation γ produced within the near-wall regions through the production term P^γ and the Coriolis term C^γ into the core regions. The large magnitude of the transportation term T^γ assures the sufficient sustaining of the secondary flows in the core regions. In our previous work,[10] we show the previous profile distributions of the secondary flows with relatively large Reynolds numbers $Re_\tau = 1000$ and 2000. The typical characteristics of the secondary flows are first present within the near-wall regions and then gradually develop into the core regions. The dominant wall-normal transportation provides an alternative explanation for the developing process of the secondary flows. With higher rotation numbers, the magnitudes of all budget terms increase, especially within the near-wall regions. The role of the Coriolis term C^γ is more apparent above the buffer layers, with the

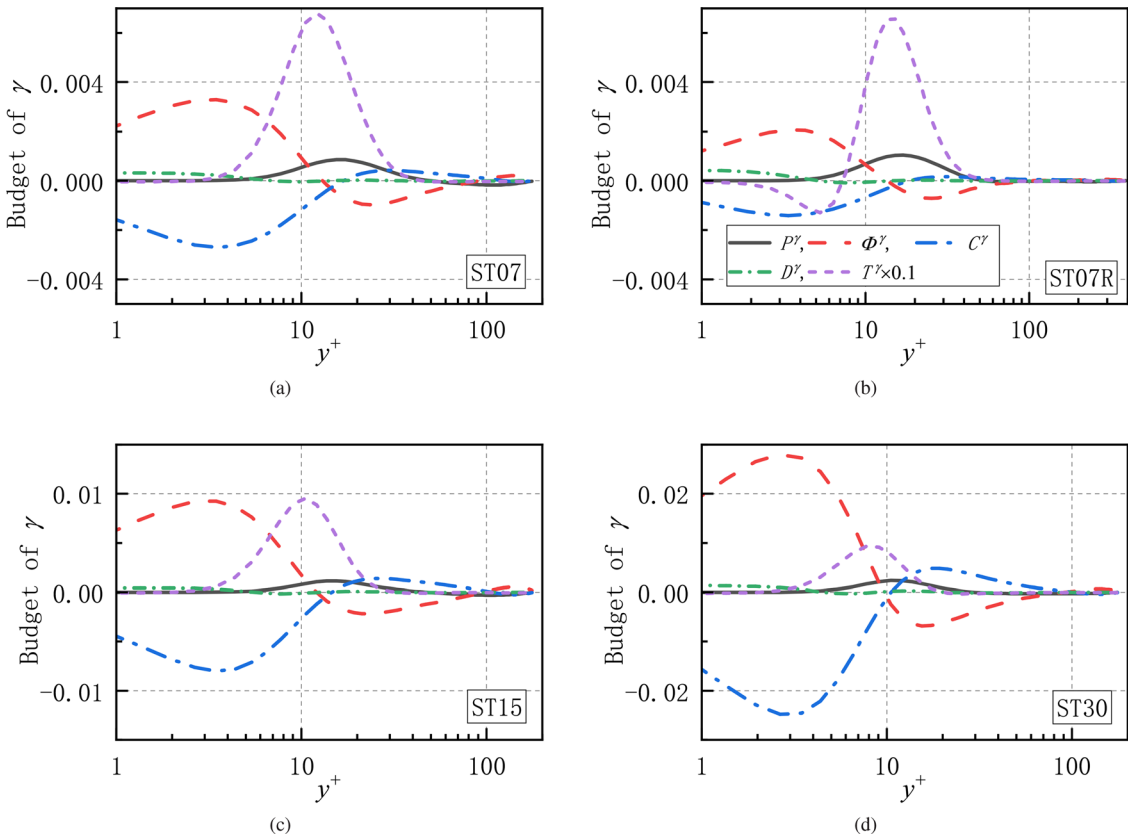

FIG. 7. Profiles of the budget terms of the mean velocity–vorticity correlation γ with different rotation numbers and Reynolds numbers. The magnitudes of the transportation term T^γ are relatively large, and we show 10% of their magnitudes for a visual comparison. (a) ST07, (b) ST07R, (c) ST15, and (d) ST30. All budget terms are non-dimensionalized by u_τ^3/δ^2 according to their dimensions.

increase in the rotation numbers. However, the dominant role of the transportation term is weakened with the increase in rotation numbers. With the increase in the Reynolds number, the magnitudes of all budget terms decrease. It can be concluded that the rotation numbers have a more important influence on the secondary flows, and the Reynolds number effects are less important, especially within the near-wall regions.

The definition of the transportation term in Eq. (12) consists of not only wall-normal gradient but also some source terms. To be mentioned, these corresponding source terms can be simplified into a wall-normal gradient form in the fluctuating helicity equation. To further investigate the statistical properties of the transportation term, we can decompose it into four terms as follows:

$$T_1^\gamma = -\frac{\partial}{\partial x_2}\left(\langle u_2'(\omega_1'u_2' - \omega_2'u_1')\rangle - \nu\frac{\partial \gamma}{\partial x_2}\right), \tag{13a}$$

$$T_2^\gamma = \left\langle \omega_k'\left(u_2'\frac{\partial u_1'}{\partial x_k} - u_1'\frac{\partial u_2'}{\partial x_k}\right)\right\rangle, \tag{13b}$$

$$T_3^\gamma = \langle\omega_1\rangle\left\langle u_2'\frac{\partial u_1'}{\partial x_1} - u_1'\frac{\partial u_2'}{\partial x_1}\right\rangle, \tag{13c}$$

$$T_4^\gamma = \langle\omega_3\rangle\left\langle u_2'\frac{\partial u_1'}{\partial x_3} - u_1'\frac{\partial u_2'}{\partial x_3}\right\rangle. \tag{13d}$$

The profiles of the above four transportation terms of ST07 are shown in Fig. 8. The numerical consequences reveal that the large magnitudes of the transportation term originate from the fourth term. The fourth term involves the mean spanwise vorticity and local spatial spanwise gradient and makes an important contribution for the total transportation term. However, the involved spanwise information would be absent in the budget of the Reynolds stress equation.

C. The mean and fluctuating helicity

Although the presence of the mean spanwise velocity and the mean streamwise vorticity characterizes the secondary flows, the non-zero mean streamwise velocity and corresponding mean spanwise vorticity are weakened by the presence of system rotation.[2–4,9] Hence, the combination of all directional velocities and vorticities might provide a more comprehensive description of the secondary flows. Previous studies indicate that the mean and fluctuating helicity is an alternative description method,[36,37,39,41,58] which could represent the combined effects of affected velocities and vorticities by system rotation.

Setting $i = j$, we can obtain the mean and fluctuating helicity as

$$H = \langle u_i\rangle\langle\omega_i\rangle, \quad h = \langle u_i'\omega_i'\rangle. \tag{14}$$

The numerical results of the mean and fluctuating helicity with different rotation numbers and Reynolds numbers are shown in Figs. 9 and 10, respectively, and their profile distributions can also characterize the secondary flows, similar to the profile distributions of

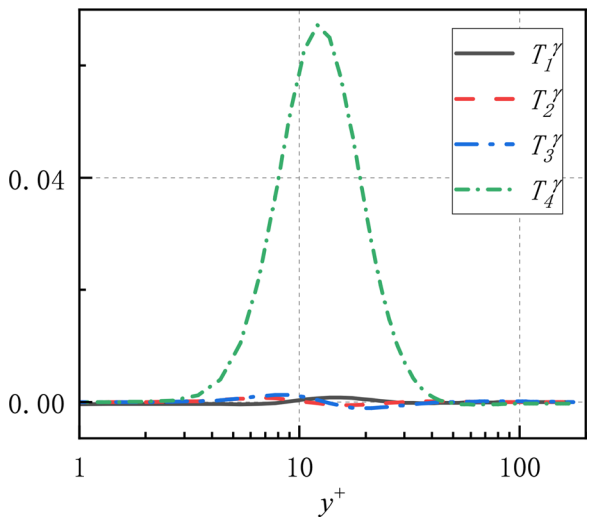

FIG. 8. Profiles of the four transportation terms of ST07.

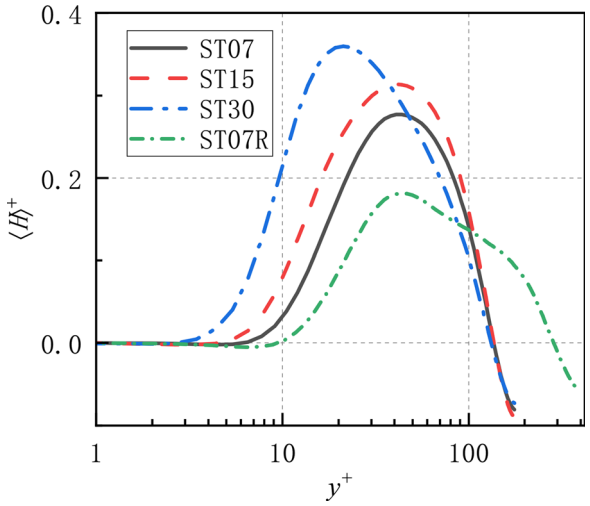

FIG. 9. Profiles of the mean helicity with different rotation numbers and Reynolds numbers.

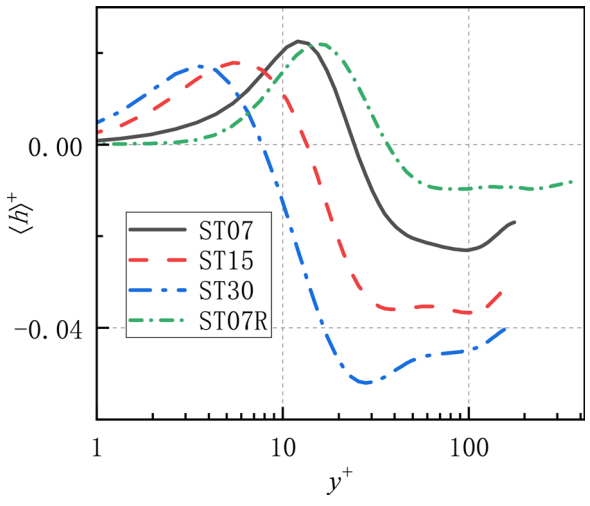

FIG. 10. Profiles of the fluctuating helicity with different rotation numbers and Reynolds numbers.

the mean spanwise velocity and the mean streamwise vorticity. More specific discussions of the profile distributions of the mean and fluctuating helicity could refer to our previous paper.[10]

The governing equations of the mean and fluctuating helicity with a steady state can be obtained as

$$\frac{\partial H}{\partial t} = 0 = \underbrace{\langle u_i' u_2' \rangle \frac{\partial \langle \omega_i \rangle}{\partial x_2} + \left(\langle u_2' \omega_i' \rangle - \langle u_i' \omega_2' \rangle \right) \frac{\partial \langle u_i \rangle}{\partial x_2}}_{P^H} \underbrace{-2\nu \frac{\partial \langle u_i \rangle}{\partial x_2} \frac{\partial \langle \omega_i \rangle}{\partial x_2}}_{D^H} \underbrace{- \frac{\Pi}{\rho} \langle \omega_1 \rangle}_{\chi^H} \underbrace{- \frac{\partial}{\partial x_2} \left(\langle u_i' u_2' \rangle \langle \omega_i \rangle + \left(\langle u_2' \omega_i' \rangle - \langle u_i' \omega_2' \rangle \right) \langle u_i \rangle - \nu \frac{\partial H}{\partial x_2} \right)}_{T^H} \quad (i = 1, 3 \quad \text{and} \quad i \neq 2), \tag{15}$$

$$\frac{\partial h}{\partial t} = 0 = \underbrace{- \langle u_i' u_2' \rangle \frac{\partial \langle \omega_i \rangle}{\partial x_2} - \left(\langle u_2' \omega_i' \rangle - \langle u_i' \omega_2' \rangle \right) \frac{\partial \langle u_i \rangle}{\partial x_2}}_{P^h} \underbrace{- \frac{1}{\rho} \left\langle \frac{\partial p'}{\partial x_i} \omega_i' \right\rangle}_{\Phi^h} \underbrace{-2\Omega_1 \langle \varepsilon_{i1l} u_l' \omega_i' \rangle}_{C^h} \underbrace{-2\nu \left\langle \frac{\partial u_i'}{\partial x_k} \frac{\partial \omega_i'}{\partial x_k} \right\rangle}_{D^h} \underbrace{- \frac{\partial}{\partial x_2} \left(\langle u_i' \omega_i' u_2' \rangle - \nu \frac{\partial h}{\partial x_2} \right) + \left\langle \omega_2' u_i' \frac{\partial u_i'}{\partial x_2} \right\rangle}_{T^h}. \tag{16}$$

The governing equation of the mean helicity [Eq. (15)] indicates that the mean pressure gradient driving the flows also makes an important contribution, in addition to the Reynolds stresses, helical stresses, and viscous term present in Eqs. (5) and (10). The pressure term is not involved in the budget of the mean helicity, and it differs from the mean helicity in the Ekman boundary layer.[5,12,59] Similar to Secs. III A and III B, the Coriolis term only appears in the fluctuating helicity equation, which reflects an indirect influence on the secondary flows. The production term serves as a bridge between the mean and fluctuating helicity, which mainly transfers helicity from the mean fields into the fluctuating fields above the buffer layer.

The production term for the mean helicity in Eq. (15) is important to be investigated, and it is also involved in the governing equation of the fluctuating helicity in Eq. (16). Hence, we select the governing equation of the fluctuating helicity to explore the budget of the secondary flows from the perspective of the helicity evolution. The budget terms of the fluctuating helicity with different rotation numbers and Reynolds numbers are shown in Fig. 11. Similar to the production term P^γ of the mean velocity–vorticity correlation γ in Fig. 7, the sign of the production term P^h is always negative. Nevertheless, the fluctuating helicity is positive within the near-wall and negative above the buffer layers. Hence, the production term P^h plays a sink role in the near-wall regions and source role above the buffer layers. The profile distribution characteristics of the production term P^h for the fluctuating helicity are combined results of the production term P_{23}^R for the Reynolds stress $\langle u_2' u_3' \rangle$ and the production term P^γ for the mean velocity–vorticity correlation γ. The pressure term plays a source role in the total sense, and there exists a position delay with the total fluctuating helicity. The role of the Coriolis term is opposite to the role of the pressure term with a smaller magnitude. Part of the pressure is induced by the Coriolis term,[57] and the combined effect of the pressure and Coriolis terms is represented on the source role for the evolution of the fluctuating helicity. In contrast to the very large wall-normal transportation of the mean velocity–vorticity correlation γ, the spatial transportation of the fluctuating helicity is comparable to other budget terms. The sign of the transportation term T^h is almost opposite to the fluctuating helicity. The wall-normal transportation role to sustain the high helicity distribution in the core regions is also confirmed. The rotation number effects are also reflected on the larger magnitudes of the budget terms and smaller wall-normal positions of the peaks. The Reynolds number effects are also reflected on the smaller magnitudes.

The production term can be further decomposed into two components, according to the involved velocity deformation and vorticity deformation fields. We denote the coupling of the Reynolds stress and vorticity deformation as the first term P_1^h and also denote the coupling of the helical stress and velocity deformation as the second term P_2^h. Their definitions are

$$P_1^h = - \langle u_i' u_2' \rangle \frac{\partial \langle \omega_i \rangle}{\partial x_2}, \quad P_2^h = - \left(\langle u_2' \omega_i' \rangle - \langle u_i' \omega_2' \rangle \right) \frac{\partial \langle u_i \rangle}{\partial x_2}. \tag{17}$$

We show the first and second production terms with different rotation numbers and Reynolds numbers in Fig. 12. The second terms are always dominant, in contrast to the first terms. The second term involves the helical stress present in the fluctuating vorticity equation, and it means that the velocity–vorticity correlation makes an essential contribution to the secondary flows. Under a weak rotation condition, the sign of the first term is opposite to the second term. With the increase in the rotation numbers, the first production term changes from positive values into negative values to be consistent with the sign of the second production term. The sign transfer of the first production term corresponds to the source or sink role for the fluctuating helicity evolution, and it uncovers an alternative physical mechanism for the secondary flows from the perspective of Reynolds stress. The opposite role of the first production term is more apparent with a higher Reynolds number.

IV. CONCLUSIONS

In this paper, we investigate the streamwise system rotation effects in turbulent channel flows from three perspectives. We conclude that the helicity could also be used to describe the streamwise system rotation effects, including the secondary flows and weakened dominant velocity and vorticity.

The first perspective to characterize the secondary flows is the mean spanwise velocity. The Reynolds stress $\langle u_2' u_3' \rangle$ is the only source term present in the governing equation of the mean spanwise velocity. This perspective has been investigated in previous work,[28] and the production term is regarded as an alternative self-sustaining mechanism for the secondary flows. The second perspective is through the analysis of the mean streamwise vorticity. It corresponds to the wall-normal gradient of the mean spanwise velocity, and its governing equation involves helical stress. The helical stress consists of velocity–vorticity correlation $\gamma = \langle \omega_1' u_2' \rangle - \langle u_1' \omega_2' \rangle$, and its profile distribution shows a different statistical characteristic in contrast to the Reynolds stress involved in the first perspective. With the increase in the wall-normal distance, the magnitude of the velocity–vorticity correlation γ increases to a peak value

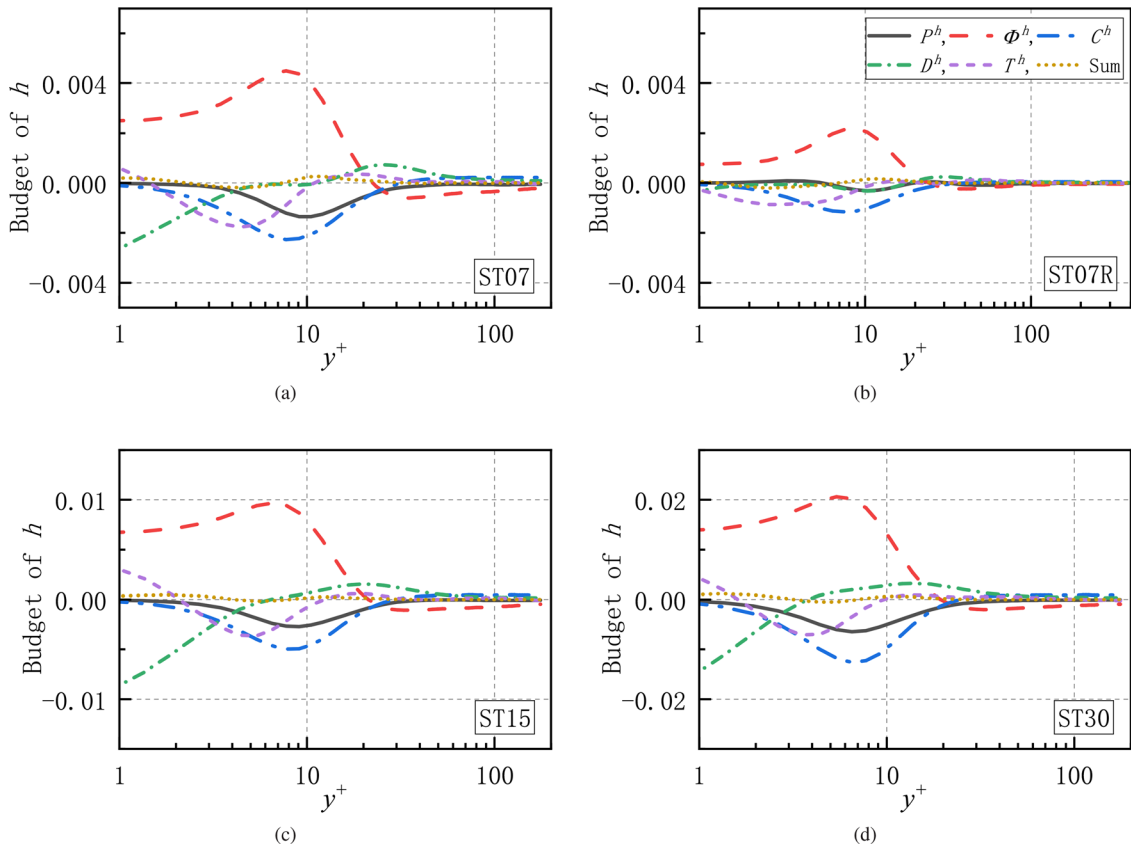

FIG. 11. Profiles of the budget terms of the fluctuating helicity with different rotation numbers and Reynolds numbers. (a) ST07, (b) ST07R, (c) ST15, and (d) ST30. All budget terms are non-dimensionalized by u_τ^3/δ^2 according to their dimensions.

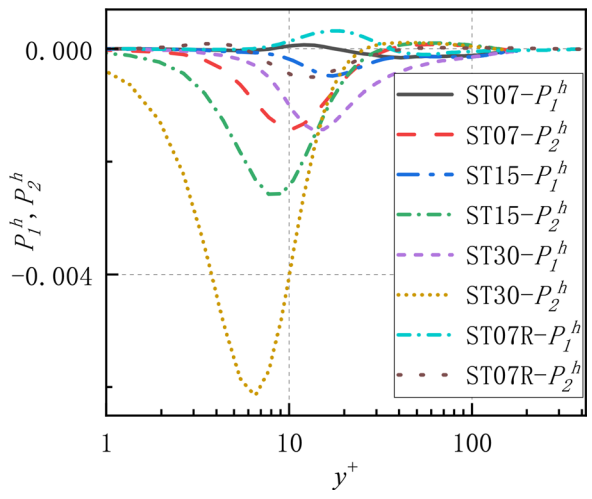

FIG. 12. Profiles of the production terms with different rotation numbers and Reynolds numbers.

first until around the buffer layer and then decreases. The peak location is slightly below the buffer layer, which is consistent with the peak value of the mean helicity. The budget of the velocity–vorticity correlation γ indicates that the production term serves as a sink term, in contrast to the complex role of the production term for Reynolds stress $\langle u_2' u_3' \rangle$. However, the statistical characteristic of the pressure term is more complex. The magnitude of the wall-normal transportation term is relatively large, which transfers the helicity produced within the near-wall regions into the core regions along the wall-normal direction.

The third perspective to characterize the secondary flows is to analyze the mean and fluctuating helicity. The mean and fluctuating helicity definitions determine that they are combined results of the affected velocity and vorticity induced by the system rotation, and helicity serves as a comprehensive investigation method of the secondary flows. Their governing equations reveal that the production term is a bridge between the mean and fluctuating fields. For the budget of the fluctuating helicity, even the sign of the production term is always negative. Its role for the fluctuating helicity evolution is different. It plays a sink role within the near-wall regions and is a source role above the buffer layer. The production term could be further decomposed into

two terms, which originates from Reynolds stress and helical stress, respectively. The second production term originating the coupling of the helical stress and velocity deformation is dominant, derived from the fluctuating vorticity equation. The combined pressure and Coriolis terms play a source role, which provides a visual explanation of the system rotation effect on the origin of the secondary flows.

Characterizing the streamwise system rotation effects in turbulent channel flows from the perspective of helicity budget can be summarized as three aspects. The first is that the helicity itself is a combined effect of velocity and vorticity. The system rotation effects are represented on all directional velocities and vorticities, and only velocity or vorticity investigation might be insufficient to explore the secondary flows. The second is that the origin and sustaining mechanisms of the secondary flows are more comprehensive. The combined pressure and Coriolis terms induced by the system rotation play a source role to explain the origin of the secondary flows. The production terms involving the helical stress provide a sustaining mechanism, and the transportation term transfers the produced helicity within the near-wall regions into the core regions. The last is that helicity itself is a conservative value, which determines the system evolution.[36–38,45,47]

The rotation number effects are reflected on the larger magnitudes and smaller peak locations of the focused values. The Reynolds number effects are slightly weak within the scope of the current numerical simulations.

ACKNOWLEDGMENTS

This work was supported by the National Key Research and Development Program of China (Nos. 2019YFA0405300 and 2020YFA0711800) and the National Natural Science Foundation of China (NSFC Grants Nos. 12072349 and 91852203). The authors thank the National Supercomputer Center in Tianjin (NSCC-TJ) and the National Supercomputer Center in GuangZhou (NSCC-GZ) for providing computer time. In addition, we would like to express our honest appreciation to Professor Yang Zixuan for his generosity in providing in-house numerical simulation codes.

AUTHOR DECLARATIONS

Conflict of Interest

The authors have no conflicts to disclose.

Author Contributions

Yan Zheng: Data curation (lead); Software (equal); writing – original draft (lead). **Li Xinliang:** Supervision (equal). **Yu Changping:** Writing – review & editing (equal).

DATA AVAILABILITY

The data that support the findings of this study are available from the corresponding author upon reasonable request.

APPENDIX: THE GOVERNING EQUATIONS OF THE MEAN AND FLUCTUATING VELOCITY–VORTICITY CORRELATION TERMS

Basing on the mean and fluctuating momentum and vorticity equations, we derive the mean velocity–vorticity correlation term $H_{ij} = \langle u_i \rangle \langle \omega_j \rangle$ and the fluctuating velocity–vorticity correlation term $h_{ij} = \langle u_i' \omega_j' \rangle$ as follows:

$$\frac{\partial H_{ij}}{\partial t} = \underbrace{\langle u_i' u_k' \rangle \frac{\partial \langle \omega_j \rangle}{\partial x_k} + \left(\langle u_k' \omega_j' \rangle - \langle u_j' \omega_k' \rangle \right) \frac{\partial \langle u_i \rangle}{\partial x_k}}_{P_{ij}^H} \underbrace{- \frac{1}{\rho} \frac{\partial \langle p \rangle}{\partial x_i} \langle \omega_j \rangle}_{\Phi_{ij}^H} \underbrace{- 2\varepsilon_{ikl} \Omega_k \langle u_l \rangle \langle \omega_j \rangle + 2\Omega_k \langle u_i \rangle \frac{\partial \langle u_j \rangle}{\partial x_k}}_{C_{ij}^H} \underbrace{- 2\nu \frac{\partial \langle u_i \rangle}{\partial x_k} \frac{\partial \langle \omega_j \rangle}{\partial x_k}}_{D_{ij}^H}$$
$$\underbrace{- \frac{\Pi}{\rho} \delta_{i1} \langle \omega_j \rangle}_{\chi_{ij}^H} \underbrace{- \frac{\partial}{\partial x_k} \left(\langle u_k \rangle H_{ij} + \langle u_i' u_k' \rangle \langle \omega_j \rangle + \left(\langle u_k' \omega_j' \rangle - \langle u_j' \omega_k' \rangle \right) \langle u_i \rangle - \nu \frac{\partial H_{ij}}{\partial x_k} \right) + \langle \omega_k \rangle \langle u_i \rangle \frac{\partial \langle u_j \rangle}{\partial x_k}}_{T_{ij}^H}, \tag{A1}$$

$$\frac{\partial h_{ij}}{\partial t} = \underbrace{- \langle u_i' u_k' \rangle \frac{\partial \langle \omega_j \rangle}{\partial x_k} - \left(\langle u_k' \omega_j' \rangle - \langle u_j' \omega_k' \rangle \right) \frac{\partial \langle u_i \rangle}{\partial x_k}}_{P_{ij}^h} \underbrace{- \frac{1}{\rho} \left\langle \frac{\partial p'}{\partial x_i} \omega_j' \right\rangle}_{\Phi_{ij}^h} \underbrace{- \langle 2\varepsilon_{ikl} \Omega_k u_l' \omega_j' \rangle + 2\Omega_k \left\langle u_i' \frac{\partial u_j'}{\partial x_k} \right\rangle}_{C_{ij}^h} \underbrace{- 2\nu \left\langle \frac{\partial u_i'}{\partial x_k} \frac{\partial \omega_j'}{\partial x_k} \right\rangle}_{D_{ij}^h}$$
$$\underbrace{- \frac{\partial}{\partial x_k} \left(\langle u_k \rangle h_{ij} + \langle u_i' \omega_j' u_k' \rangle - \nu \frac{\partial h_{ij}}{\partial x_k} \right) + \left\langle \omega_k' u_i' \frac{\partial u_j'}{\partial x_k} \right\rangle + \langle \omega_k \rangle \left\langle u_i' \frac{\partial u_j'}{\partial x_k} \right\rangle}_{T_{ij}^h}. \tag{A2}$$

REFERENCES

[1] P. Bradshaw, "Turbulent secondary flows," Annu. Rev. Fluid Mech. **19**, 53–74 (1987).
[2] H. Wu and N. Kasagi, "Effects of arbitrary directional system rotation on turbulent channel flow," Phys. Fluids **16**, 979–990 (2004).
[3] M. Oberlack, W. Cabot, B. A. P. Reif, and T. Weller, "Group analysis, direct numerical simulation and modelling of a turbulent channel flow with streamwise rotation," J. Fluid Mech. **562**, 383–403 (2006).
[4] A. Pouquet and P. D. Mininni, "The interplay between helicity and rotation in turbulence: Implications for scaling laws and small-scale dynamics," Philos. Trans. R. Soc. London, Ser. A **368**, 1635–1662 (2010).
[5] E. Deusebio and E. Lindborg, "Helicity in the Ekman boundary layer," J. Fluid Mech. **755**, 654–671 (2014).
[6] I. Recktenwald, T. Weller, W. Schröder, and M. Oberlack, "Comparison of direct numerical simulations and particle-image velocimetry data of turbulent

channel flow rotating about the streamwise axis," Phys. Fluids **19**, 085114 (2007).
[7]Y. T. Yang, W. D. Su, and J. Z. Wu, "Helical-wave decomposition and applications to channel turbulence with streamwise rotation," J. Fluid Mech. **662**, 91–122 (2010).
[8]Z. X. Yang and B. C. Wang, "Capturing Taylor–Görtler vortices in a streamwise-rotating channel at very high rotation numbers," J. Fluid Mech. **838**, 658–689 (2018).
[9]Y. J. Dai, W. X. Huang, and C. X. Xu, "Coherent structures in streamwise rotating channel flow," Phys. Fluids **31**, 021204 (2019).
[10]C. P. Yu, R. N. Hu, Z. Yan, and X. L. Li, "Helicity distributions and transfer in turbulent channel flows with streamwise rotation," J. Fluid Mech. **940**, A18 (2022).
[11]B. Y. Li, N. S. Liu, and X. Y. Lu, "Direct numerical simulation of wall-normal rotating turbulent channel flow with heat transfer," Int. J. Heat Fluid Flow **49**, 1162–1175 (2006).
[12]O. G. Chkhetiani, M. V. Kurgansky, and N. V. Vazaeva, "Turbulent helicity in the atmospheric boundary layer," Boundary Layer Meteorol. **168**, 361–385 (2018).
[13]C. Bergmann and B. C. Wang, "Direct numerical simulation of turbulent heat transfer in a wall-normal rotating channel flow," Int. J. Heat Fluid Flow **80**, 108480 (2019).
[14]N. S. Liu and X. Y. Lu, "A numerical investigation of turbulent flows in a spanwise rotating channel," Comput. Fluids **36**, 282–298 (2007).
[15]Y. T. Yang and J. Z. Wu, "Channel turbulence with spanwise rotation studied using helical wave decomposition," J. Fluid Mech. **692**, 137–152 (2012).
[16]Z. H. Xia, Y. P. Shi, and S. Y. Chen, "Direct numerical simulation of turbulent channel flow with spanwise rotation," J. Fluid Mech. **788**, 42–56 (2016).
[17]Z. Jiang, Z. H. Xia, Y. P. Shi, and S. Y. Chen, "Large eddy simulation of spanwise rotating turbulent channel flow with dynamic variants of eddy viscosity model," Phys. Fluids **30**, 040909 (2018).
[18]X. L. Huang, X. I. A. Yang, and R. F. Kunz, "Wall-modeled large-eddy simulations of spanwise rotating turbulent channels-comparing a physics-based approach and a data-based approach," Phys. Fluids **31**, 125105 (2019).
[19]Y. Xia, Z. S. Yu, and Y. Guo, "Interface-resolved numerical simulations of particle-laden turbulent channel flows with spanwise rotation," Phys. Fluids **32**, 013303 (2020).
[20]N. Alkishriwi, M. Meinke, and W. Schröder, "Large-eddy simulation of streamwise-rotating turbulent channel flow," Comput. Fluid **37**, 786–792 (2008).
[21]X. L. Huang and X. I. A. Yang, "A Bayesian approach to the mean flow in a channel with small but arbitrarily directional system rotation," Phys. Fluids **33**, 015103 (2021).
[22]L. Marstorp, G. Brethouwer, O. Grundestam, and A. V. Johansson, "Explicit algebraic subgrid stress models with application to rotating channel flow," J. Fluid Mech. **639**, 403–432 (2009).
[23]B. C. Wang and D. J. Bergstrom, "A dynamic nonlinear subgrid-scale stress model," Phys. Fluids **17**, 035109 (2005).
[24]B. C. Wang and Y. Zhang, "Large-eddy simulation of turbulent flows in a heated streamwise rotating channel," Int. J. Heat Mass Transfer **44**, 71–86 (2013).
[25]Q. Q. Xun, B. C. Wang, and E. Yee, "Large-eddy simulation of turbulent heat convection in a spanwise rotating channel flow," Int. J. Heat Mass Transfer **54**, 698–716 (2011).
[26]J. Yin, B. C. Wang, and D. J. Bergstrom, "Large-eddy simulation of combined forced and natural convection in a vertical plane channel," Int. J. Heat Mass Transfer **50**, 3848–3861 (2007).
[27]I. Recktenwald, N. Alkishriwi, and W. Schröder, "PIV-LES analysis of channel flow rotating about the streamwise axis," Eur. J. Mech.—B/Fluids **28**, 677–688 (2009).
[28]Z. X. Yang, B. Q. Deng, B. C. Wang, and L. Shen, "On the self-constraint mechanism of the cross-stream secondary flow in a streamwise-rotating channel," Phys. Fluids **32**, 105115 (2020).
[29]R. C. Chin, R. Vinuesa, R. Örlü, J. I. Cardesa, A. Noorani, M. S. Chong, and P. Schlatter, "Backflow events under the effect of secondary flow of Prandtl's first kind," Phys. Rev. Fluids **5**, 074606 (2020).
[30]T. J. Hüttl and R. Friedrich, "Direct numerical simulation of turbulent flows in curved and helically coiled pipes," Comput. Fluids **30**, 591–605 (2001).
[31]A. Noorani, G. K. E. Khoury, and P. Schlatter, "Evolution of turbulence characteristics from straight to curved pipes," Int. J. Heat Fluid Flow **41**, 16–26 (2013).
[32]S. Pirozzoli, D. Modesti, P. Orlandi, and F. Grasso, "Turbulence and secondary motions in square duct flow," J. Fluid Mech. **840**, 631–655 (2018).
[33]D. Modesti, S. Pirozzoli, P. Orlandi, and F. Grasso, "On the role of secondary motions in turbulent square duct flow," J. Fluid Mech. **847**, R1 (2018).
[34]P. Orlandi and S. Pirozzoli, "Turbulent flows in square ducts: Physical insight and suggestions for turbulence modellers," J. Turbul. **21**, 106–128 (2020).
[35]A. Brissaud, "Helicity cascades in fully developed isotropic turbulence," Phys. Fluids **16**, 1366–1367 (1973).
[36]H. K. Moffatt and A. Tsinober, "Helicity in laminar and turbulence flow," Annu. Rev. Fluid Mech. **24**, 281–312 (1992).
[37]Q. N. Chen, S. Y. Chen, G. L. Eyink, and D. D. Holm, "Intermittency in the joint cascade of energy and helicity," Phys. Rev. Lett. **90**, 214503 (2003).
[38]A. Pouquet and N. Yokoi, "Helical fluid and (Hall)-MHD turbulence: A brief review," Philos. Trans. R. Soc. London, Ser. A **380**, 20210087 (2022).
[39]H. K. Moffatt, "Degree of knottedness of tangled vortex lines," J. Fluid Mech. **35**, 117–129 (1969).
[40]H. K. Moffatt, "Helicity-invariant even in a viscous fluid," Science **357**, 448–449 (2017).
[41]Z. Yan, X. L. Li, C. P. Yu, J. C. Wang, and S. Y. Chen, "Dual channels of helicity cascade in turbulent flows," J. Fluid Mech. **894**, R2 (2020).
[42]Q. Nguyen and D. V. Papavassiliou, "Using helicity to investigate scalar transport in wall turbulence," Phys. Rev. Fluids **5**, 062601 (2020).
[43]L. Biferale, S. Musacchio, and F. Toschi, "Inverse energy cascade in three-dimensional isotropic turbulence," Phys. Rev. Lett. **108**, 164501 (2012).
[44]A. Alexakis, "Helically decomposed turbulence," J. Fluid Mech. **812**, 752–770 (2017).
[45]A. Alexakis and L. Biferale, "Cascades and transitions in turbulent flows," Phys. Rep. **767–769**, 1–101 (2018).
[46]Z. Yan, X. Li, Y. Fu, and C. Yu, "The effect of helicity on kinetic energy cascade in compressible helical turbulence," Adv. Appl. Math. Mech. **11**, 700–710 (2019).
[47]Z. Yan, X. L. Li, J. C. Wang, and C. P. Yu, "Effect of pressure on joint cascade of kinetic energy and helicity in compressible helical turbulence," Phys. Rev. E **99**, 033114 (2019).
[48]Z. Yan, X. L. Li, C. P. Yu, and J. C. Wang, "Cross-chirality transfer of kinetic energy and helicity in compressible helical turbulence," Phys. Rev. Fluids **5**, 084604 (2020).
[49]Z. X. Yang, B. Q. Deng, B. C. Wang, and L. Shen, "Sustaining mechanism of Taylor–Görtler-like vortices in a streamwise-rotating channel flow," Phys. Rev. Fluids **5**, 044601 (2020).
[50]N. N. Mansour, J. Kim, and P. Moin, "Reynolds-stress and dissipation-rate budgets in a turbulent channel flow," J. Fluid Mech. **194**, 15–44 (1988).
[51]S. Hoyas and J. Jiménez, "Reynolds number effects on the Reynolds-stress budgets in turbulent channels," Phys. Fluids **20**, 101511 (2008).
[52]T. Kawata and P. H. Alfredsson, "Inverse interscale transport of the Reynolds shear stress in plane Couette turbulence," Phys. Rev. Lett. **120**, 244501 (2018).
[53]C. I. Chan, P. Schlatter, and R. Chin, "Interscale transport mechanisms in turbulent boundary layers," J. Fluid Mech. **921**, A13 (2021).
[54]G. K. Vallis, *Atmospheric and Oceanic Fluid Dynamics* (Cambridge University Press, 2017).
[55]J. Kim, P. Moin, and R. Moser, "Turbulence statistics in fully-developed channel flow at low Reynolds number," J. Fluid Mech. **177**, 133–166 (1987).
[56]S. B. Pope, *Turbulent Flows* (IOP Publishing, 2001).
[57]Z. X. Yang, B. Q. Deng, B. C. Wang, and L. Shen, "The effects of streamwise system rotation on pressure fluctuations in a turbulent channel flow," Phys. Fluids **30**, 091701 (2018).
[58]R. B. Pelz, V. Yakhot, S. A. Orszag, L. Shtilman, and E. Levich, "Velocity–vorticity patterns in turbulent flow," Phys. Rev. Lett. **54**, 2505–2508 (1985).
[59]A. Ojha, M. Anas, A. Ranjan, P. Joshi, and M. K. Verma, "Helicity segregation by Ekman pumping in laminar rotating flows with gravity orthogonal to rotation," Phys. Rev. Fluids **7**, 034801 (2022).